IEEE Access
Multidisciplinary ⋮ Rapid Review ⋮ Open Access Journal

Received April 3, 2021, accepted April 8, 2021, date of publication April 14, 2021, date of current version July 1, 2021.

Digital Object Identifier 10.1109/ACCESS.2021.3073074

Command Filter Adaptive Power Capture Control Based on Fuzzy Rules Emulated Networks for Variable Speed Wind Turbines With Flexible Shaft

MIAO HUANG, LILI TAO, AND ZHIHUA HU
College of Intelligent Manufacturing and Control Engineering, Shanghai Polytechnic University, Shanghai 201209, China
Corresponding author: Miao Huang (huangmiao@sspu.edu.cn)

This work was supported in part by the National Nature Science Foundation of China under Grant 62003205 and Grant 61673268, in part by the Zhejiang Provincial Natural Science Foundation of China under Grant LQ19F030005, and in part by the Natural Science Foundation of Ningbo under Grant 2019A610092 and Grant 2019C50026.

ABSTRACT This paper considers the power capture control problem of variable-speed wind turbine (VSWT) systems with flexible shaft. The control objective is to optimize the capture of wind energy by tracking the desired power output. A novel command filter based adaptive power signal feedback (PSF) control method is proposed to design the PSF controller for the non-affine nonlinear VSWT systems with a two-mass model for which the parameters are totally unknown. A compensation dynamic with adaptable parameters is designed to compensate the errors caused by command filtering and the unknown control gains. The unavailable aerodynamic torque is approximated by introducing fuzzy rules emulated networks (FRENs) and estimations of the unknown parameters and their learning laws are established to derive the virtual and actual control laws. Meanwhile, it is proved that all the signals in the closed-loop system are uniformly ultimately bounded (UUB) via Lyapunov synthesis. Finally, the feasibility of the proposed controllers is demonstrated on a 5-MW variable-speed wind turbine.

INDEX TERMS Adaptive control, fuzzy rules emulated networks, nonlinear control systems, wind energy generation.

I. INTRODUCTION

With the growing atmospheric pollution and the energy crisis caused by the shortage of traditional fossil fuels, the use of clean and renewable energy sources, such as wind energy, has received widely attention. Wind Energy Conversion Systems (WECSs) convert wind energy into electricity and their main components are wind turbines. Wind turbines include fixed speed wind turbines (FSWT) and variable speed wind turbines (VSWT). When the wind speed is less than the rated wind speed, the VSWT is able to vary the turbine rotational speed along with the wind speed changes, obtaining the maximum possible power. Since wind turbines operate below rated wind speeds for a significant portion of their service life, the VSWT system captures a significant amount of additional energy. As a result, most new installations are of the variable speed type ([1]).

The wind turbine drive train dynamic consists of components that convert the rotational kinetic energy driven by the wind into electrical energy, which is the component with highest failure rates in wind turbines. Therefore, ensuring the reliability of the drive train is critical to reduce wind turbine downtime. As the power and size of a wind turbine increases, so does the force and torque required, resulting a greater torsional behaviour in the driveline. Most existing dynamic models consider concentrated single-mass drive-train dynamics, ignoring the effects of all torsional behaviour on the turbine dynamic responses. To this end, a two-mass model with flexible shaft is considered in [2]–[4] to describe the drive train dynamic of the wind turbines for explaining the overall dynamic response of the wind turbines, as well as the design and maintenance of its internal driveline components.

The associate editor coordinating the review of this manuscript and approving it for publication was Ahmed F. Zobaa.

The maximum power point tracking (MPPT) problem is to maximize the wind energy capture when a VSWT system is operating in the lower speed band (i.e., between the cut-in wind speed and the rated wind speed) and is a critical control issue for improving wind energy capture efficiency using a VSWT such as [5]–[9]. Commonly used control methods are: Tip Speed Ratio(TSR) control, Optimal Torque(OT) control, Power Signal Feedback(PSF) control and Perturb and Observation (P&O) methods. PSF control is developed on the basis of OT control, the main different from PSF with OT is the feedback signal and reference signal are the active power instead of the torque.

Conventional PSF controllers designed in [10]–[14] usually use look-up tables or data-driven methods to achieve the maximum energy extraction. However, these methods require accurate mathematical models or large amounts of field data and are difficult to implement. [15], [16] try to enhance the transient and steady-state performances by feedback linearization and error transformation methods, respectively. Nevertheless, these methods are designed for concentrated single-mass transmission system dynamics, dynamic effects of the PSF method on the flexible shaft driven VSWT system have not been addressed in existing literature.

During the past decade, lots of nonlinear control methods have been proposed and applied to the electrical power systems ([17]–[21]). To solve the complexity explosion problem caused by the repeated differentiation of the virtual control signal in back-stepping control methods, dynamic surface control involves a first-order filtering for the virtual control input to substitute the differential of the virtual control input at each step of the back-stepping design([22]–[26]). On the basis of the dynamic surface control methods, back-stepping control schemes based on command filtering are proposed, which introduce a set of dynamic compensation signals to reduce the errors caused by the filtering ([27]–[35]). In [34], fuzzy logic systems are employed to approximate nonlinear uncertainties, which has been used for reference in this paper.

In this paper, we propose a novel command filter based adaptive PSF control method for flexible shaft driven VSWT systems with totally unknown parameters to deal with the power capture control problem. To compensate the command filtering error and unknown control gains, a compensation dynamic with adaptable parameters has been established. Meanwhile, fuzzy rules emulated networks (FRENs) have been introduced to estimate the unavailable nonlinear dynamics in controller design. The main contributions of this article are listed as follows:

- Comparing with the current results on command filter adaptive control method proposed by [27]–[32], [34] which are designed for affine nonlinear systems, the proposed control method can deal with the non-affine nonlinear VSWT systems.
- Unlike [27], [29]–[31] require known control gains, the virtual and actual control gains of the considered systems are totally unknown, so a new error compensation dynamic has been established with the estimation of the virtual control gain.
- FRENs established by [36] are firstly utilized in continuous-time command filter adaptive control systems to approximate the unavailable aerodynamic torque without assuming its boundedness or it satisfied the Lipschitz condition, which are required in [27], [29], [30], [33].

The remainder of this paper is organized as follows. Section II describes the dynamics of VSWT and formulates the control problem. In Section III, the detailed command filter adaptive controller design method with FRENs is provided. Section IV presents the stability analysis and the uniformly ultimately boundedness of the proposed closed-loop system is proved. Simulation results for a 5-MW VSWT with applying the proposed controller are given in Section V. Finally, some conclusions are given in the last section.

II. PROBLEM STATEMENT

The VSWT systems considered here are composed of a direct drive generator and a wind turbine as depicted in Figure 1. The excitation of common generators is replaced by the permanent magnet in permanent magnet synchronous generators which have the advantages of simple and reliable structure, lower excitation power and higher power generation efficiency. To improve the efficiency and the power density, as well as reduce maintenance requirements of the system, a design without a gearbox which has a high pole-number and enables wind turbines to rotate at 20-40r/min has been applied. However, this paper does not specify a particular generator technology.

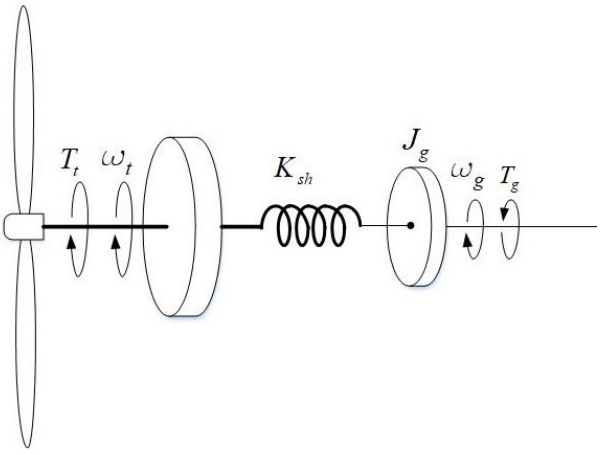

FIGURE 1. Drive train dynamics.

Considering that the turbine and the generator are connected by a flexible shaft and their lumped inertias are separated, the two-mass model presented by [2] has been firstly introduced to describe the drive-train dynamic.

The system dynamic is given by

$$\dot{\omega}_g = \frac{K_{sh}}{J_g}\theta_{sh} - \frac{1}{J_g}T_g \tag{1}$$

$$\dot{\theta}_{sh} = \omega_t - \omega_g \tag{2}$$

$$\dot{\omega}_t = -\frac{K_{sh}}{J_t}\theta_{sh} + \frac{1}{J_t}T_t \tag{3}$$

$$P_g = T_g\omega_g \tag{4}$$

where the state variables ω_t, θ_{sh} and ω_g represent the rotational speed of the turbine, the torsional displacement of the shaft and the rotational speed of the generator, respectively. T_g denotes the electromagnetic torque of the generator. K_{sh} is the shaft stiffness constant, J_t and J_g denote inertias of the turbine and generator, respectively. The output power available from the generator is defined as P_g. The aerodynamic torque of turbine T_t is a nonlinear function specified by

$$T_t = \frac{1}{2}\rho C_p(\lambda, \beta_\lambda)\pi R^5 \frac{1}{\lambda^3}\omega_t^2, \lambda = \frac{\omega_t R}{v} \tag{5}$$

where ρ and R are the air density and the radius of the turbine blade. v denotes the wind velocity. C_p is the power coefficient, depends on the blade pitch angle β_λ and the tip-speed ratio λ. The power coefficient surfaces for the wind turbine considered in this work are obtained using the blade-element moment theory implemented in a wind turbine performance code (WT-PERF [37]) developed by NREL.

Remark 1: In [38], six-mass, three-mass, and two-mass drive-train models are adopted to analyze the transient behavior of VSWT systems. The two-mass model is reduced from the six-mass model in which the friction forces of individual masses are considered. In the process of simplification, the friction forces between the hub and blades, the shaft and the generator, the shaft and the turbine are neglected. The conclusion is given that the two-mass shaft model is sufficient, with reasonable accuracy, for the transient stability analysis of VSWT systems.

The operating state of the turbines can be divided into two major regions. In Low speed region, the wind speed v satisfies $v_{rated} > v \geq v_{cut-in}$ and the turbine power is lower than the rated power. In High speed region, it has $v_{cut-off} > v \geq v_{rated}$ and the turbine power equals the rated power, where v_{cut-in}, $v_{cut-off}$ and v_{rated} represent the cut-in, the cut-off and the rated wind speed, respectively.

The control problem concerned in this work is to maximize the turbine power in Low speed region. The mechanical power extracted by the turbine from wind is a function of C_p:

$$P_a = \frac{1}{2}\rho\pi R^2 C_p(\lambda, \beta_\lambda)v^3. \tag{6}$$

Since for any tip-speed ratio λ, $C_p(\lambda, \beta_\lambda)$ is maximize when it has $\beta_\lambda = 0\,\text{deg}$ in Low speed region and for a fixed β_λ, there exists an optimal tip-speed ratio λ_{opt} corresponding to a unique maximum C_{pmax} of $C_p(\lambda, \beta_\lambda)$. Therefore, the maximum amount of the energy a turbine can capture in the wind can be obtained as

$$P_{amax} = \frac{1}{2}\rho\pi R^2 C_{pmax} v^3. \tag{7}$$

In application, the grid frequency control requires an energy buffer to cope with sudden consumption changes, so it is preferable to operate the turbine at a power which is slightly lower than the maximum. Therefore, the control objective of this work is to design the generator torque T_g so that the output power P_g of the generator can track the reference power $P_d = n_p P_{amax}$, $0 < n_p < 1$, in the situation that all the parameters in the system are unknown and ensure that all the signals in the closed-loop are uniformly ultimately bounded. The definition of uniformly ultimately bounded is presented as follows which is given by [39]:

Definition 1: Let $V(x)$ be a Lyapunov candidate function and suppose that the set S is compact. The solutions of $\dot{x} = f(t, x)$ are uniformly ultimately bounded (UUB) if there exist β and γ and for every $0 < \tau < \gamma$ and $\delta = \delta(\tau, \beta) \geq 0$ such that $\|x(t_0)\| \leq \tau \Rightarrow \|x(t)\| \leq \beta, \forall t \geq t_0 + \delta$. Then, there exists $V(x)$ which satisfies $\dot{V}(x) \leq -\epsilon\|x\|^2$, where $\epsilon > 0$.

III. CONTROLLER DESIGN

In this section, an adaptive PSF controller based on the command filter back-stepping control method is design to adjust the output power P_g to track the reference power P_d. The controller design process is divided into two parts. Firstly, the command filter and error compensation dynamic are defined. Secondly, the back-stepping controller with adaptive parameters is derived. The details of each part are as follows.

A. COMMAND FILTER AND ERROR COMPENSATION DYNAMIC

To trace the reference signal P_d, coordinate transformation is required. Let $z_1 = T_g\omega_g - P_d$, $z_2 = T_g\theta_{sh} - \bar{\alpha}_2$ and $z_3 = T_g\omega_t - \bar{\alpha}_3$. $\bar{\alpha}_i$ is the output of the first-order command filter with respect to the virtual controller α_i, $i = 2, 3$, which are defined as

$$\varepsilon_2\dot{\bar{\alpha}}_2 + \bar{\alpha}_2 = \alpha_1, \tag{8}$$

$$\varepsilon_3\dot{\bar{\alpha}}_3 + \bar{\alpha}_3 = \alpha_2, \tag{9}$$

$$\bar{\alpha}_i(0) = \alpha_{i-1}(0), \tag{10}$$

where ε_i are positive constants to be designed.

According to the system dynamic (4), the dynamic of the state vector $z = [z_1, z_2, z_3]^T$ can be derived.

$$\dot{z}_1 = \dot{T}_g\omega_g + gz_2 + g(\bar{\alpha}_2 - \alpha_1) + g\alpha_1 - \frac{T_g^2}{J_g} - \dot{P}_d \tag{11}$$

$$\dot{z}_2 = \theta_{sh}\dot{T}_g + T_g(\omega_t - \omega_g) - \dot{\bar{\alpha}}_2 = \theta_{sh}\dot{T}_g - T_g\omega_g + z_3 + (\bar{\alpha}_3 - \alpha_2) + \alpha_2 - \dot{\bar{\alpha}}_2 \tag{12}$$

$$\dot{z}_3 = \dot{T}_g\omega_g + T_g\dot{\omega}_t - \dot{\bar{\alpha}}_3 = \dot{T}_g\omega_t - T_g\frac{K_{sh}}{J_t}\theta_{sh} + \frac{T_g T_t}{J_t} - \dot{\bar{\alpha}}_3. \tag{13}$$

where $g = \frac{K_{sh}}{J_g}$, which is a unknown control gain. Let $\hat{g} \in R$ is the estimated parameter of g.

Remark 2: It can be seen that the transformation dynamic (11)-(13) doesn't satisfy the affine nonlinear form such as $\dot{z} = f(z) + g(z)u$, in which the primary term of the control signal must be separated from the states.

To eliminate the effect of the errors $(\bar{\alpha}_i - \alpha_{i-1}), i = 2, 3$ introduced by the command filter in (8)-(10), define signals $\xi_i, i = 1, 2, 3$ as follows:

$$\begin{aligned}\dot{\xi}_1 &= -l_1 sign(\xi_1) - k_1\xi_1 \\ &\quad + \hat{g}(k)\left(\xi_2 + (\bar{\alpha}_2 - \alpha_1)\right) \quad (14)\\ \dot{\xi}_2 &= -l_2 sign(\xi_2) - k_2\xi_2 + \bar{\alpha}_3 - \alpha_2 + \xi_3 \quad (15)\\ \dot{\xi}_3 &= -l_3 sign(\xi_3) - k_3\xi_3 \quad (16)\\ \xi_i(0) &= \xi_{i0}, i = 1, 2, 3, \quad (17)\end{aligned}$$

where $l_i > 0, k_i > 0, i = 1, 2, 3$ are the designed parameters, ξ_{i0} are the initial conditions.

Define the compensated tracking errors as

$$s_i = z_i - \xi_i, i = 1, 2, 3. \quad (18)$$

By plugging (11)-(13) and (14)-(15) into (18), we have

$$\begin{aligned}\dot{s}_1 &= \dot{T}_g\omega_g + gz_2 + g\left(\bar{\alpha}_2 - \alpha_1\right) + g\alpha_1 + l_1 sign(\xi_1) \\ &\quad -\frac{T_g^2}{J_g} - \dot{P}_d - \hat{g}\xi_2 - \hat{g}\left(\bar{\alpha}_2 - \alpha_1\right) + k_1\xi_1 \\ &= \dot{T}_g\omega_g + gs_2 - \tilde{g}\xi_2 - \tilde{g}(\bar{\alpha}_2 - \alpha_1) + g\alpha_1 \\ &\quad + l_1 sign(\xi_1) + k_1\xi_1 - \frac{T_g^2}{J_g} - \dot{P}_d \quad (19)\\ \dot{s}_2 &= \theta_{sh}\dot{T}_g + T_g\omega_g + z_3 - \xi_3 + (\bar{\alpha}_3 - \alpha_2) + \alpha_2 - \dot{\bar{\alpha}}_2 \\ &\quad - (\bar{\alpha}_3 - \alpha_2) + k_2\xi_2 + l_2 sign(\xi_2) \\ &= \theta_{sh}\dot{T}_g + T_g\omega_g + s_3 + \alpha_2 \\ &\quad - \dot{\bar{\alpha}}_2 + k_2\xi_2 + l_2 sign(\xi_2) \quad (20)\\ \dot{s}_3 &= \dot{T}_g\omega_t - T_g\frac{K_{sh}}{J_t}\theta_{sh} + \frac{T_gT_t}{J_t} \\ &\quad -\dot{\bar{\alpha}}_3 + k_3\xi_3 + l_3 sign(\xi_3), \quad (21)\end{aligned}$$

where $\tilde{g} = \hat{g} - g$ is the estimation error of $\hat{g}$.

B. ADAPTIVE BACK-STEPPING CONTROLLER DESIGN WITH FRENs

The control design divides in 3 steps.

Step 1: It is obvious that applying aerodynamic torque T_t formed by mechanism modelling to controller design for an actual turbine will increase uncertainty.

Moreover, from the definition of P_d, we have $\dot{P}_d = \frac{3}{2}n_p\rho\pi R^2 C_{pmax}v\dot{v}$, which means that the measurement of $\dot{v}$ should be implemented when the explicit form of $\dot{P}_d$ is applied to the controller. It will obviously lead to the increment of the cost and additional measurement noise.

To overcome this drawback, ANNs based estimator was implemented to approximate T_t and $\dot{P}_d$ in [16]. However, the ANNs' structure and adjustable parameters are usually set up randomly. In this work, T_t and $\dot{P}_d$ are referred as unknown terms to be estimated by FRENs whose structure and adjustable parameters are designed in the sense of engineering not in the random aspect([40]).

To this end, the unknown T_t and $\dot{P}_d$ are approximated with idea parameters and rewritten as

$$T_t = \beta_T^T\varphi_T \quad (22)$$

$$\dot{P}_d = -\beta_d^T\varphi_d \quad (23)$$

where $\varphi_T \in R^{m_T}$ and $\varphi_d \in R^{m_d}$ are regression vectors and $\beta_T \in R^{m_T}$ and $\beta_d \in R^{m_d}$ are unknown parameters of the regression vectors. In this work, the regression vectors will be established by a set of membership functions of FRENs to cover operating range of s_1 and s_3 with the numbers of membership m_T and m_d for T_t and $\dot{P}_d$, respectively.

Let $\hat{T}_t = \hat{\beta}_T^T\varphi_T$ and $\hat{\dot{P}}_d = \hat{\beta}_d^T\varphi_d$ be the estimations of T_t and $\dot{P}_d$, where $\hat{\beta}_T \in R^{m_T}$ and $\hat{\beta}_d \in R^{m_d}$ are the adjustable parameter vectors and their learning law will be designed below.

Example 1: The following is an example of using the IF-THEN rules to establish the estimation of T_t when m_T are both set up to 7.

IF s_1 is NL THEN $\hat{T}_{t1} = \hat{\beta}_{T1}\mu_{NL}(s_3)$
IF s_1 is NM THEN $\hat{T}_{t2} = \hat{\beta}_{T2}\mu_{NM}(s_3)$
IF s_1 is NS THEN $\hat{T}_{t3} = \hat{\beta}_{T3}\mu_{NS}(s_3)$
IF s_1 is Z THEN $\hat{T}_{t4} = \hat{\beta}_{T4}\mu_{Z}(s_3)$
IF s_1 is PS THEN $\hat{T}_{t5} = \hat{\beta}_{T5}\mu_{PS}(s_3)$
IF s_1 is PM THEN $\hat{T}_{t6} = \hat{\beta}_{T6}\mu_{PM}(s_3)$
IF s_1 is PL THEN $\hat{T}_{t7} = \hat{\beta}_{T7}\mu_{PL}(s_3)$

The estimation of $T_t(\cdot)$ can be obtained as

$$\hat{T}_t = \sum_{i=1}^{7}\hat{T}_{ti} = \hat{\beta}_T^T\varphi_T, \quad (24)$$

where $\hat{\beta}_T = [\hat{\beta}_{T1}, \cdots, \hat{\beta}_{T7}]^T$ is the adjustable parameter vector, $\varphi = [\mu_{NL}, \mu_{NM}, \mu_{NS}, \mu_Z, \mu_{PS}, \mu_{PM}, \mu_{PL}]^T$ and $\mu_{NL}, \mu_{NM}, \mu_{NS}, \mu_Z, \mu_{PS}, \mu_{PM}, \mu_{PL}$ are membership functions of s_3. The architecture of $\hat{T}_t$ shows in Figure 2.

Let $\hat{\beta}_1$ be the estimation of the unknown parameter vector $\beta_1 = [-\frac{1}{J_g}, \beta_d^T]^T$ and $\varphi_1 = [T_g^2, \varphi_d^T]^T$. To derive the virtual control signal, we define a quadratic function $V_1 = \frac{1}{2}s_1^2 + \frac{1}{2r_1}\tilde{\beta}_1^T\tilde{\beta}_1 + \frac{1}{2r_g}\tilde{g}^2$, where $\tilde{\beta}_1 = \hat{\beta}_1 - \beta_1$ is the estimation error of $\hat{\beta}_1$, r_1 and r_g are the designed positive constants. The derivative of V_1 is given as

$$\begin{aligned}\dot{V}_1 &= s_1\left(\dot{T}_g\omega_g + gs_2 - \tilde{g}\xi_2 - \tilde{g}(\bar{\alpha}_2 - \alpha_1) + g\alpha_1\right. \\ &\quad \left. + l_1 sign(\xi_1) + k_1\xi_1 + \beta_1^T\varphi_1\right) + \frac{1}{r_1}\tilde{\beta}_1^T\dot{\hat{\beta}}_1 + \frac{1}{r_g}\tilde{g}\dot{\hat{g}} \\ &\le s_1\left(\dot{T}_g\omega_g + gs_2 + g\alpha_1 + \beta_1^T\varphi_1 + k_1\xi_1 + l_1 sign(\xi_1)\right) \\ &\quad - s_1\left(\tilde{g}\xi_2 + \tilde{g}(\bar{\alpha}_2 - \alpha_1)\right) + \frac{1}{r_1}\tilde{\beta}_1^T\dot{\hat{\beta}}_1 + \frac{1}{r_g}\tilde{g}\dot{\hat{g}} \\ &\le s_1\left(\dot{T}_g\omega_g + \hat{g}s_2 + \hat{g}\alpha_1 + k_1\xi_1 + \hat{\beta}_1^T\varphi_1 + l_1 sign(\xi_1)\right) \\ &\quad - s_1\tilde{g}\left(z_2 + \bar{\alpha}_2\right) - s_1\tilde{\beta}_1^T\varphi_1 + \frac{1}{r_1}\tilde{\beta}_1^T\dot{\hat{\beta}}_1 + \frac{1}{r_g}\tilde{g}\dot{\hat{g}}. \quad (25)\end{aligned}$$

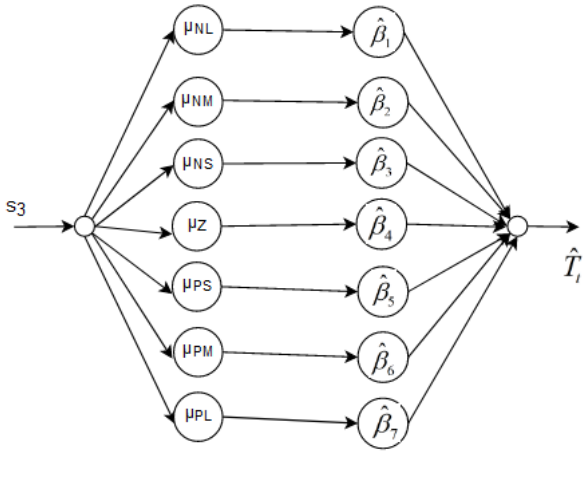

FIGURE 2. The architecture of FRENs $\hat{T}_t$.

Design the update law of the estimated parameters $\hat{g}$ and $\hat{\beta}_1$ as follows:

$$\dot{\hat{g}} = -r_g\hat{g} + r_g s_1 (z_2 + \bar{\alpha}_2), \hat{g}(0) = \hat{g}_0 \tag{26}$$

$$\dot{\hat{\beta}}_1 = -r_1\hat{\beta}_1 + r_1 s_1\varphi_1, \hat{\beta}_1(0) = \hat{\beta}_{10}. \tag{27}$$

where $k_1/2 > r_g > 0$, $r_1 > 0$ are positive design parameters, $\hat{g}_0 \in R$ and $\hat{\beta}_{10} \in R^{m_d}$ are the initial values of $\hat{g}$ and $\hat{\beta}_1$. Let the virtual control signal α_1 satisfy

$$\alpha_1 = -\frac{\hat{g}(k)\Gamma_1}{r_g + \left\|\hat{g}(k)\right\|^2}, \tag{28}$$

where $\Gamma_1 = k_1 z_1 + \hat{\beta}_1^T\varphi_1 + l_1 sign(\xi_1)$. Therefore,

$$\dot{V}_1 \le s_1\dot{T}_g\omega_g + \hat{g}s_1 s_2 - \Upsilon_1 s_1^2 + \Upsilon_g\Gamma_1^2 - \tilde{\beta}_1^T\hat{\beta}_1 - \tilde{g}\hat{g}, \tag{29}$$

where $\Upsilon_g = \frac{2r_g}{(r_g+\|\hat{g}(k)\|^2)^2} > 0$ and $\Upsilon_1 = k_1 - 2r_g > 0$.

Step 2:

Let $V_2 = V_1 + \frac{1}{2}s_2^2$ and derivative of V_2 can be given by:

$$\begin{aligned}\dot{V}_2 &= \dot{V}_1 + s_2\dot{s}_2\\ &\le s_1\dot{T}_g\omega_g + \hat{g}s_1 s_2 - \Upsilon_1 s_1^2 + \Upsilon_g\Gamma_1^2\\ &\quad - \tilde{\beta}_1^T\hat{\beta}_1 - \tilde{g}\hat{g} + s_2\left(\theta_{sh}\dot{T}_g + T_g\omega_g + s_3 + \alpha_2\right.\\ &\quad \left.-\dot{\bar{\alpha}}_2 + k_2\xi_2 + l_2 sign(\xi_2)\right)\\ &\le s_1\dot{T}_g\omega_g + s_2\dot{T}_g\theta_{sh} - \Upsilon_1 s_1^2 + \Upsilon_g\Gamma_1^2\\ &\quad + s_2\left(\alpha_2 + k_2\xi_2 + T_g\omega_g + \hat{g}s_1 - \dot{\bar{\alpha}}_2\right.\\ &\quad \left.+ l_2 sign(\xi_2)\right) - \tilde{\beta}_1^T\hat{\beta}_1 + s_2 s_3 - \tilde{g}\hat{g}.\end{aligned} \tag{30}$$

Let

$$\alpha_2 = -k_2 z_2 - T_g\omega_g + \dot{\bar{\alpha}}_2 - l_2 sign(\xi_2) - \hat{g}s_1. \tag{31}$$

Inequality (30) can be reduced to

$$\begin{aligned}\dot{V}_2 \le s_1\dot{T}_g\omega_g + s_2\dot{T}_g\theta_{sh} + s_2 s_3 - \sum_{i=1}^{2}\Upsilon_i s_i^2\\ - \tilde{\beta}_1^T\hat{\beta}_1 - \tilde{g}\hat{g} + \Upsilon_g\Gamma_1^2\end{aligned} \tag{32}$$

where $\Upsilon_2 = k_2$.

Step 3:

Let $\beta_2 = [-\frac{K_{sh}}{J_t}, \frac{\beta_T^T}{J_t}]^T$, $\varphi_2 = [\theta_{sh}T_g, T_g\varphi_T^T]^T$, $\hat{\beta}_2 \in R^{m_T+1}$ be the estimation of β_2 and $\tilde{\beta}_2 = \hat{\beta}_2 - \beta_2 \in R^{m_T+1}$ be the estimation error. Define $V_3 = V_2 + \frac{1}{2}s_3^2 + \frac{1}{2r_2}\tilde{\beta}_2^T\tilde{\beta}_2$. Then,

$$\begin{aligned}\dot{V}_3 &\le s_1\dot{T}_g\omega_g + s_2\dot{T}_g\theta_{sh} + s_3\dot{T}_g\omega_t\\ &\quad + s_3\left(s_2 - \dot{\bar{\alpha}}_3 + \beta_2^T\varphi_2 + k_3\xi_3 + l_3 sign(\xi_3)\right)\\ &\quad - \sum_{i=1}^{2}\Upsilon_i s_i^2 - \tilde{\beta}_1^T\hat{\beta}_1 + \frac{1}{r_2}\tilde{\beta}_2^T\dot{\hat{\beta}}_2 - \tilde{g}\hat{g} + \Upsilon_g\Gamma_1^2\\ &\le s_1\dot{T}_g\omega_g + s_2\dot{T}_g\theta_{sh} + s_3\dot{T}_g\omega_t - \sum_{i=1}^{2}\Upsilon_i s_i^2 - \tilde{\beta}_1^T\hat{\beta}_1\\ &\quad + s_3\left(s_2 - \dot{\bar{\alpha}}_3 + \hat{\beta}_2^T\varphi_2 + k_3\xi_3 + l_3 sign(\xi_3)\right)\\ &\quad + \Upsilon_g\Gamma_1^2 - s_3\tilde{\beta}_2^T\varphi_2 + \frac{1}{r_2}\tilde{\beta}_2^T\dot{\hat{\beta}}_2 - \tilde{g}\hat{g}.\end{aligned} \tag{33}$$

Let the dynamics of $\dot{\hat{\beta}}_2$ and control signal T_g be designed as

$$\dot{\hat{\beta}}_2 = -r_2\hat{\beta}_2 + r_2\varphi_2 s_3, \hat{\beta}_2(0) = \hat{\beta}_{20} \tag{34}$$

$$\dot{T}_g = -\frac{\delta_u\Gamma_2}{r_u + \|\delta_u\|^2}, T_g(0) = T_{g0} \tag{35}$$

where $\delta_u = s_1\omega_g + s_2\theta_{sh} + s_3\omega_t$ and $\Gamma_2 = s_3\left(s_2 - \dot{\bar{\alpha}}_3 + z_3 k_3 + \hat{\beta}_2^T\varphi_2 + l_3 sign(\xi_3)\right) + \Upsilon_g\Gamma_1^2$, $r_2 > 0$, $r_u > 0$ are design parameters. $\hat{\beta}_{20} \in R^{m_t+1}$ and T_{g0} are the initial values of $\hat{\beta}_2$ and T_g.

Then, we have

$$\begin{aligned}\dot{V}_3 \le \sum_{i=1}^{3}\left(-\Upsilon_i s_i^2\right) - \tilde{\beta}_1^T\hat{\beta}_1 - \tilde{\beta}_2^T\hat{\beta}_2 - \tilde{g}\hat{g}\\ + \Upsilon_u\Gamma_2^2 + 2r_u.\end{aligned} \tag{36}$$

where $\Upsilon_3 = k_3$ and $\Upsilon_u = \frac{2r_u}{(r_u+\|\delta_u\|^2)^2} > 0$.

In summary, the dynamics of virtual control signal $\alpha_i, i = 1, 2$ and control signal T_g are generated by (28), (31)and (35), and rewritten as follows

$$\alpha_1 = -\frac{\hat{g}(k)(k_1 z_1 + \hat{\beta}_1^T\varphi_1 + l_1 sign(\xi_1))}{r_g + \left\|\hat{g}(k)\right\|^2}, \tag{37}$$

$$\alpha_2 = -k_2 z_2 + T_g\omega_g + \dot{\bar{\alpha}}_2 - l_2 sign(\xi_2) - \hat{g}s_1, \tag{38}$$

$$\dot{T}_g = -\frac{\delta_u}{r_u + \|\delta_u\|^2}\left(s_3\left(s_2 - \dot{\bar{\alpha}}_3 + z_3 k_3 + \hat{\beta}_2^T\varphi_2\right.\right.$$
$$\left.\left.+ l_3 sign(\xi_3)\right) + \Upsilon_g\Gamma_1^2\right). \tag{39}$$

where $\delta_u = s_1\omega_g + s_2\theta_{sh} + s_3\omega_t$, $\Upsilon_g = \frac{2r_g}{(r_g+\|\hat{g}(k)\|^2)^2} > 0$ **and** $\Gamma_1 = k_1 z_1 + \hat{\beta}_1^T\varphi_1 + l_1 sign(\xi_1)$.

The structure of the proposed close-loop control system is given by Figure 3.

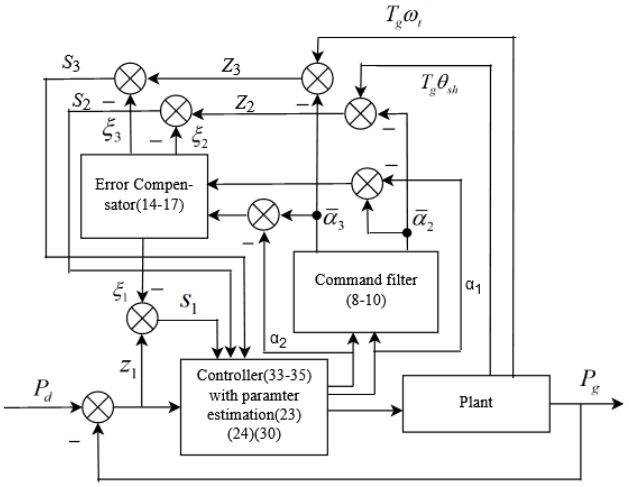

FIGURE 3. The structure of the proposed control system.

IV. STABILITY ANALYSIS

Proposition 1: Signals $\xi_i(t), i = 1, 2, 3$ defined in (14)-(16) are asymptotically convergent, if $|\bar{\alpha}_j - \alpha_{j-1}| \leq \eta_{j-1}, j = 2, 3$ and the estimation parameter $\hat{g}$ is bounded, where $\eta_{j-1} > 0$.

proof 1: Construct the following Lyapunov function

$$V_4 = \sum_{i=1}^{3} \frac{1}{2}\xi_i^2. \tag{40}$$

Taking the derivative of V_4, we have

$$\begin{aligned}
\dot{V}_4 &= \xi_1\dot{\xi}_1 + \xi_2\dot{\xi}_2 + \xi_3\dot{\xi}_3 \\
&= \xi_1\left(-l_1 sign(\xi_1) - k_1\xi_1 + \hat{g}\left(\xi_2 + (\bar{\alpha}_2 - \alpha_1)\right)\right) \\
&\quad + \xi_2\left(-l_2 sign(\xi_2) - k_2\xi_2 + \bar{\alpha}_3 - \alpha_2 + \xi_3\right) \\
&\quad + \xi_3\left(-l_3 sign(\xi_3) - k_3\xi_3\right)) \\
&\leq -k_1\xi_1^2 + \hat{g}\xi_1\xi_2 + \xi_1\hat{g}\left(\bar{\alpha}_2 - \alpha_1\right) - l_1|\xi_1| \\
&\quad - l_2|\xi_2| - k_2\xi_2^2 + \xi_2\left(\bar{\alpha}_3 - \alpha_2\right) \\
&\quad + \xi_2\xi_3 - k_3\xi_3^2 - l_3|\xi_3| \\
&\leq -\left(k_1 - |\hat{g}/2|\right)\xi_1^2 - \left(k_2 - |\hat{g}/2| - 1/2\right)\xi_2^2 \\
&\quad - \left(k_3 - 1/2\right)\xi_3^2 - \left(l_1 - |\hat{g}\eta_1|\right)|\xi_1| \\
&\quad - (l_2 - \eta_2)|\xi_2| - l_3|\xi_3|
\end{aligned} \tag{41}$$

Let $k_1 - |\hat{g}/2| > 0$, $k_2 - |\hat{g}/2| - 1/2 > 0$, $k_3 - 1/2 > 0$, $l_1 - |\hat{g}\eta_1| > 0$ and $l_2 - \eta_2 > 0$. Then, by integrating the left and the right sides of (41) on $[t_0, t)$, we can obtain

$$\lim_{t\to\infty} V_4(t) \leq V_4(t_0) < \infty. \tag{42}$$

Moreover, together with the boundedness of signals $\xi_i(t)$ and $(\bar{\alpha}_i - \alpha_{i-1})$, it is easy to show that $\dot{\xi}_i$ are also bounded. In view of the Barballat Lemma [41], one can verify that

$$\lim_{t\to\infty} \xi_i = 0, \quad i = 1, 2, 3 \tag{43}$$

that is, the asymptotic convergence is achieved. This completes the proof.

Theorem 1: For the uncertain VSWT system characterized by (1)-(4), if the adaptive controller composes of the virtual control laws (28) and (31), the actual control law (35), the command filter (8)-(10), the error compensation dynamic (14)-(16) and the update laws of adaptive parameters(26), (27) and (34). Then, all signals of the closed-loop system are UUB.

proof 2: By the definitions of $\tilde{\beta}_j, j = 1, 2$ and $\tilde{g}$ completing the squares, one has

$$\begin{aligned}
-\tilde{\beta}_j^T\hat{\beta}_j &= -\tilde{\beta}_j^T\left(\beta_j + \tilde{\beta}_j\right) \\
&= -\tilde{\beta}_j^T\tilde{\beta}_j - \tilde{\beta}_j^T\beta_j \leq \frac{\beta_j^T\beta_j}{4},
\end{aligned} \tag{44}$$

$$-\tilde{g}\hat{g} = -\tilde{g}\left(g + \tilde{g}\right) = -\tilde{g}^2 - \tilde{g}g \leq \frac{g^2}{4}. \tag{45}$$

Thus, by substituting(44) and (45) into (36), one can get

$$\begin{aligned}
\dot{V}_3 &\leq -\sum_{i=1}^{3}\Upsilon_i s_i^2 + \sum_{j=1}^{2}\frac{\beta_j^T\beta_j}{4} + \frac{g^2}{4} + \Upsilon_u\Gamma_2^2 + 2r_u \\
&\leq -\sum_{i=1}^{3}\Upsilon_i s_i^2 + \Delta,
\end{aligned} \tag{46}$$

where $\Delta = \sum_{j=1}^{2}\frac{\beta_j^T\beta_j}{4} + \frac{g^2}{4} + \Upsilon_u\Gamma_2^2 + 2r_u$. Let $\epsilon \leq \Upsilon$ is a positive constant, where $\Upsilon = \min\{\Upsilon_1, \Upsilon_2, \Upsilon_3\}$. Then, it follows that

$$\dot{V}_3 \leq -\Upsilon\sum_{i=1}^{3}s_i^2 + \Delta \leq -\epsilon\sum_{i=1}^{3}s_i^2 \leq 0, \tag{47}$$

when $s_i \geq \sqrt{\frac{\Delta}{\Upsilon - \epsilon}}$.

Hence, $\dot{V}_3$ will become negative if

$$s_i \notin \Omega_s = \left\{s \mid |s| \leq \sqrt{\frac{\Delta}{\Upsilon - \epsilon}}\right\}, \quad i = 1, 2, 3. \tag{48}$$

According to the standard Lyapunov extension theorem [42], we can conclude that $s_i, = 1, 2, 3, \hat{\beta}_j, j = 1, 2$ and $\hat{g}$ are UUB.

Further, $T_g, \alpha_{j-1}, j = 2, 3$ and $z_i, i = 1, 2, 3$ are bounded owing to the boundedness of $s_i, \hat{\beta}_j, j = 1, 2$ and $\hat{g}$. Therefore, the boundedness of $\bar{\alpha}_j, j = 2, 3$ are obtained from the command filter (8)-(10). In consequence, $|\bar{\alpha}_j - \alpha_{j-1}|$ are bounded.

Then, the conditions of Proposition 1 are all satisfied and signals ξ_i are asymptotically convergent. In conclusion, all signals of the closed-loop system are UUB.

V. SIMULATION RESULTS

Numerical simulations have been performing on a 5-MW wind turbine whose data are given in Table 1. The proposed command filter based adaptive control method has been applied to verify the system performance. The considered VSWT work at realistic wind profile case has been considered in this section. The environmental parameters of the simulation are set to $\rho = 1.225\ Kg/m^3$, $C_{pmax} = 0.449$ and $n_p = 0.9$ and the initial values of the system are $\omega_g(0) = 400$, $\theta_{sh} = 1$ and $\omega_t(0) = 400$.

TABLE 1. Wind turbine characteristics.

Parameter	Value
J_t	35,328,141 $kg \cdot m^2$
J_g	5,024,406 $kg \cdot m^2$
K_{sh}	867,637,000 $N \cdot m/rad$
R	55.5 m
Rated rotor speed	12.1 rpm
Rated power	5 MW

To test the performance of the proposed method under realistic turbulent conditions, a wind profile with stochastic variations around an average wind velocity of 7 m/s is generated by the Kaimal turbulence model, shown in Figure 4.

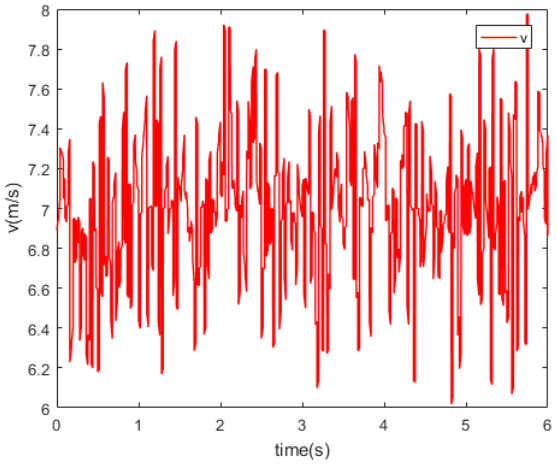

FIGURE 4. The realistic wind profile.

The parameters and initial conditions of the proposed controller are set as Table 2.

TABLE 2. Parameters and initial conditions of the proposed controller.

Parameter	Value
$\varepsilon_2, \varepsilon_3$ in Command filter (8-9)	0.05
$\bar{\alpha}_i(0) = \alpha_{i-1}(0), i = 2, 3$ in (10) ,	0
$l_i, i = 1, 2, 3$ in Error compensator (14-16)	10
$k_1 = k_3$ in (14) and (16)	120
k_2 in (15)	70
$\xi_{i0}, i = 1, 2, 3$ in (17)	0.1
$\hat{g}_0$ in (26)	170
r_g, r_1 and r_2 in (26), (27) and (34)	1
$\hat{\beta}_{10}$ in (27)	$\mathbf{0}_{8\times1}$
$\hat{\beta}_{20}$ in (34)	$\mathbf{0}_{8\times1}$
T_{g0} in (35)	0.1×10^4
The numbers m_T and m_d of φ_T and φ_d in (22) and (23)	7

Furthermore, the proposed scheme is compared with a sliding mode controller, which is implemented as $\dot{T}_g = \frac{B+5}{\omega_t}\frac{e}{|e|+1}$, where the update law of B is $\dot{B} = 100|e|$. Figure 5 shows the comparison result of the output power trajectories of the generator for the proposed command filter adaptive control system and the sliding mode control system. Figure 6 shows the torques of the generator of the two systems. The tracking errors of the two control systems are given in Figure 7.

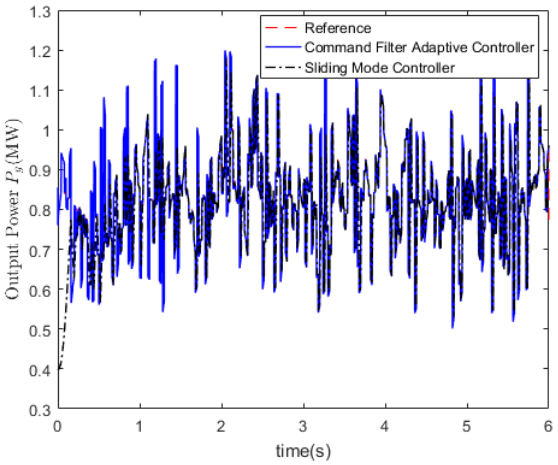

FIGURE 5. Generator output power for the case with the realistic wind profile.

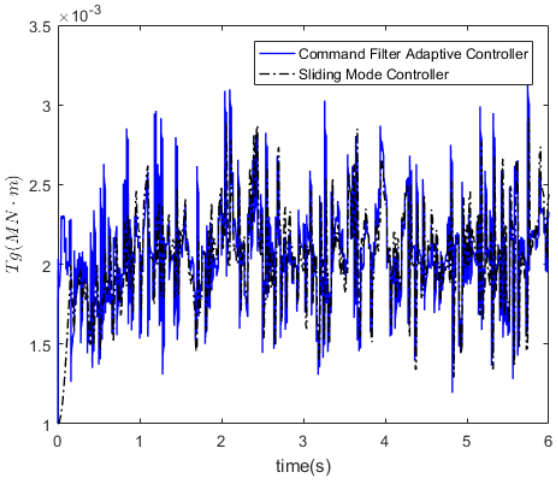

FIGURE 6. Generator torque T_g for the case with the realistic wind profile.

The result of the estimator for g is given by Figure 8. The membership functions for φ_T and φ_d in (22) and (23) are defined as Figure 9 and Figure 10, respectively, which intends the operating range to be $\pm 1MW$. Figure 11 shows $\hat{\beta}_1\varphi_1$ and $\hat{\beta}_2\varphi_2$, the outputs of the FRENs.

Given the above, the estimation errors and tracking error of the proposed control system are bounded and converge to a small neighborhood of the origin, which confirms the theoretical analysis. The mean square errors (MSEs) of the proposed control system and the sliding mode control system are $1.9918 \times 10^{-4} MW$ and $0.0124\ MW$, respectively, which implies that the advantage of the proposed control method in control accuracy.

Remark 3: Without loss of generality, the un-modeled effects in the output equation (4) of the two-mass model can be assumed as Gaussian noises, they can be estimated together with the unknown $\dot{P}_d$. To illustrate the effectiveness of the proposed control method, the Gaussian noises with the

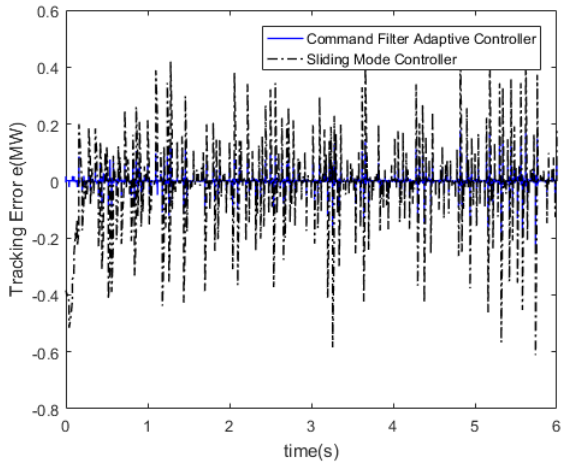

FIGURE 7. Tracking error for the case with the realistic wind profile.

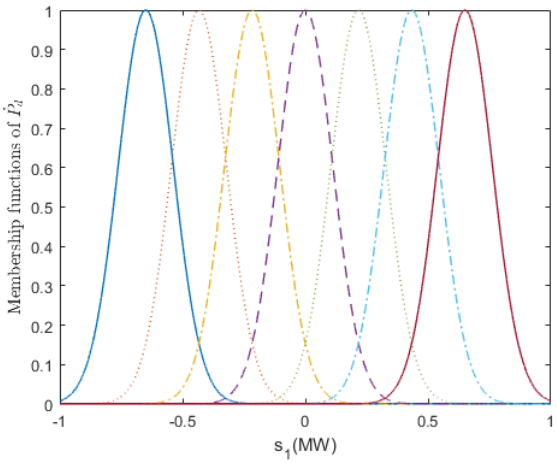

FIGURE 10. Membership functions of $\dot{P}_d$.

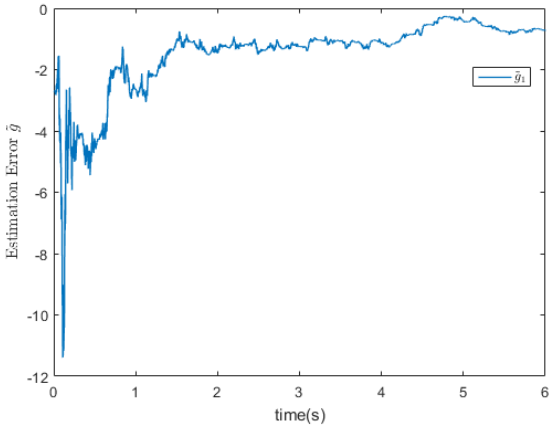

FIGURE 8. The estimation errors $\tilde{g}$ for the case with the realistic wind profile.

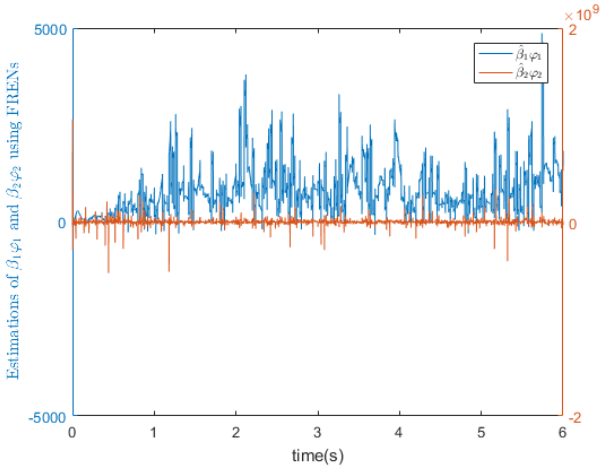

FIGURE 11. The estimations of $\beta_1\varphi_1$ and $\beta_2\varphi_2$ for the case with the realistic wind profile.

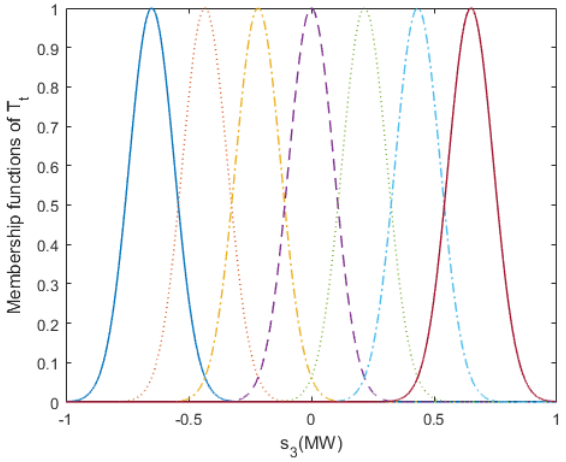

FIGURE 9. Membership functions of T_t.

standard deviation (SD) of 0.1-0.8 are added to the simulation respectively and the corresponding MSEs of the proposed control systems are listed in Table 3. Desired-trajectory-based adaptive laws which are proposed in [43], [44] can also be synthesized to compensate the model uncertainties and improve the tracking performance of adaptive control systems.

Remark 4: The system parameters listed in Table 1 are setting according to the actual parameters of a 5MW wind turbine given by [2]. The initial conditions are selected near the zero equilibrium point of the system. C_{pmax} is obtained from the performance code developed by NREL([37]). n_p is chosen the same as [16]. The control parameters are designed by the engineering experience or by many experiments. In the tuning process, one parameter will be adjusted first, while the other parameters are set to fixed values. Then, other control parameters can be adjusted one by one in the same way. The intelligent optimization algorithms can also help to guide the design parameters selection which can be regard as a multi-objective optimization problem discussed by [45].

TABLE 3. The MSEs of the proposed control system with output uncertainties.

SD of the Gaussian noise	0.1	0.2	0.3	0.4
MSE(MW)	0.0047	0.0119	0.0237	0.0402
SD of the Gaussian noise	0.5	0.6	0.7	0.8
MSE(MW)	0.0614	0.0872	0.1178	0.1530

VI. CONCLUSION

In this paper, the maximum power capture problem for the VSWT system with flexible shaft in Low-speed region is considered. A command filter adaptive PSF controller has been designed to cope with the non-affine nonlinear VSWT systems. The effects of unknown control gains and command filter has been minimized by implementing an adaptive error compensation dynamic. FRENs have been incorporated to approximate the unavailable aerodynamic torque of the VSWT system. The UUB of the proposed closed-loop system has been proved by Lyapunov synthesis and the feasibility of the controller has been demonstrated by extensive simulation studies on a 5-MW wind turbine.

Future research directions will be focused on the following points: firstly, the MPPT scheme designed to extract the maximum power in the presence of input disturbances and measurement noises, secondly, the decoupling problem of the UUB and the unknown control gain g and the unknown parameters $\beta_j, j = 1, 2$.

REFERENCES

[1] B. Feytout, P. Lanusse, J. Sabatier, and S. Gracia, "Robust CRONE design for a variable ratio planetary gearing in a variable speed wind turbine," *Asian J. Control*, vol. 15, no. 3, pp. 806–818, May 2013.

[2] K. Yenduri and P. Sensarma, "Maximum power point tracking of variable speed wind turbines with flexible shaft," *IEEE Trans. Sustain. Energy*, vol. 7, no. 3, pp. 956–965, Jul. 2016.

[3] I. P. Girsang, J. S. Dhupia, E. Muljadi, M. Singh, and L. Y. Pao, "Gearbox and drivetrain models to study dynamic effects of modern wind turbines," *IEEE Trans. Ind. Appl.*, vol. 50, no. 6, pp. 3777–3786, Nov. 2014.

[4] B. Boukhezzar and H. Siguerdidjane, "Nonlinear control of a variable-speed wind turbine using a two-mass model," *IEEE Trans. Energy Convers.*, vol. 26, no. 1, pp. 149–162, Mar. 2011.

[5] Z. Song, J. Liu, Y. Hu, Y. Cheng, and F. Tan, "Real-time performance analyses and optimal gain-scheduling control of offshore wind turbine under ice creep loads," *IEEE Access*, vol. 7, pp. 181706–181720, 2019.

[6] A. Wu, J.-F. Mao, and X. Zhang, "An ADRC-based Hardware-in-the-Loop system for maximum power point tracking of a wind power generation system," *IEEE Access*, vol. 8, pp. 226119–226130, 2020.

[7] H. Camblong, I. M. de Alegria, M. Rodriguez, and G. Abad, "Experimental evaluation of wind turbines maximum power point tracking controllers," *Energy Convers. Manage.*, vol. 47, nos. 18–19, pp. 2846–2858, Nov. 2006.

[8] L. Wang, L. Cao, and L. Zhao, "Non-linear tip speed ratio cascade control for variable speed high power wind turbines: A backstepping approach," *IET Renew. Power Gener.*, vol. 12, no. 8, pp. 968–972, 2018.

[9] X. Deng, J. Yang, Y. Sun, D. Song, Y. Yang, and Y. H. Joo, "An effective wind speed estimation based extended optimal torque control for maximum wind energy capture," *IEEE Access*, vol. 8, pp. 65959–65969, 2020.

[10] S. M. Barakati, M. Kazerani, and J. D. Aplevich, "Maximum power tracking control for a wind turbine system including a matrix converter," *IEEE Trans. Energy Convers.*, vol. 24, no. 3, pp. 705–713, Sep. 2009.

[11] L. Li, Y. Ren, J. Chen, K. Shi, and L. Jiang, "Modified P&O Approach Based Detection of the Optimal Power-Speed Curve for MPPT of Wind Turbines," in *Energy Internet*. Cham, Switzerland: Springer, 2020, pp. 137–155.

[12] V. Galdi, A. Piccolo, and P. Siano, "Designing an adaptive fuzzy controller for maximum wind energy extraction," *IEEE Trans. Energy Convers.*, vol. 23, no. 2, pp. 559–569, Jun. 2008.

[13] J. Hussain and M. K. Mishra, "Adaptive maximum power point tracking control algorithm for wind energy conversion systems," *IEEE Trans. Energy Convers.*, vol. 31, no. 2, pp. 697–705, Jun. 2016.

[14] J. E. Sierra-Garcia and M. Santos, "Improving wind turbine pitch control by effective wind neuro-estimators," *IEEE Access*, vol. 9, pp. 10413–10425, 2021.

[15] G. Hua and Y. Geng, "A novel control strategy of MPPT taking dynamics of wind turbine into account," in *Proc. 37th IEEE Power Electron. Spec. Conf.*, Jun. 2006, pp. 1–6.

[16] W. Meng, Q. Yang, Y. Ying, Y. Sun, Z. Yang, and Y. Sun, "Adaptive power capture control of variable-speed wind energy conversion systems with guaranteed transient and steady-state performance," *IEEE Trans. Energy Convers.*, vol. 28, no. 3, pp. 716–725, Sep. 2013.

[17] C. Deng, Y. Wang, C. Wen, Y. Xu, and P. Lin, "Distributed resilient control for energy storage systems in cyber–physical microgrids," *IEEE Trans. Ind. Informat.*, vol. 17, no. 2, pp. 1331–1341, Feb. 2021.

[18] B. Wang, W. Chen, J. Wang, B. Zhang, and P. Shi, "Semiglobal tracking cooperative control for multiagent systems with input saturation: A multiple saturation levels framework," *IEEE Trans. Autom. Control*, vol. 66, no. 3, pp. 1215–1222, Mar. 2021.

[19] C. Deng and C. Wen, "Distributed resilient observer-based fault-tolerant control for heterogeneous multiagent systems under actuator faults and DoS attacks," *IEEE Trans. Control Netw. Syst.*, vol. 7, no. 3, pp. 1308–1318, Sep. 2020.

[20] B. Wang, W. Chen, B. Zhang, and Y. Zhao, "Regulation cooperative control for heterogeneous uncertain chaotic systems with time delay: A synchronization errors estimation framework," *Automatica*, vol. 108, Oct. 2019, Art. no. 108486.

[21] C. Deng, W.-W. Che, and Z.-G. Wu, "A dynamic periodic event-triggered approach to consensus of heterogeneous linear multiagent systems with time-varying communication delays," *IEEE Trans. Cybern.*, vol. 51, no. 4, pp. 1812–1821, Apr. 2021.

[22] X. Shi, Y. Cheng, C. Yin, X. Huang, and S.-M. Zhong, "Design of adaptive backstepping dynamic surface control method with RBF neural network for uncertain nonlinear system," *Neurocomputing*, vol. 330, pp. 490–503, Feb. 2019.

[23] J. Yu, Y. Ma, H. Yu, and C. Lin, "Adaptive fuzzy dynamic surface control for induction motors with iron losses in electric vehicle drive systems via backstepping," *Inf. Sci.*, vol. 376, pp. 172–189, Jan. 2017.

[24] W. Zhang and W. Yi, "Fuzzy observer-based dynamic surface control for input-saturated nonlinear systems and its application to missile guidance," *IEEE Access*, vol. 8, pp. 121285–121298, 2020.

[25] Y. Zhou, W. Dong, S. Dong, Y. Chen, R. Zuo, and Z. Liu, "Robust adaptive control of MIMO pure-feedback nonlinear systems via improved dynamic surface control technique," *IEEE Access*, vol. 7, pp. 96672–96685, 2019.

[26] Y. Li, K. Li, and S. Tong, "Finite-time adaptive fuzzy output feedback dynamic surface control for MIMO nonstrict feedback systems," *IEEE Trans. Fuzzy Syst.*, vol. 27, no. 1, pp. 96–110, Jan. 2019.

[27] J. Yu, B. Chen, H. Yu, C. Lin, and L. Zhao, "Neural networks-based command filtering control of nonlinear systems with uncertain disturbance," *Inf. Sci.*, vol. 426, pp. 50–60, Feb. 2018.

[28] Y.-X. Li, "Finite time command filtered adaptive fault tolerant control for a class of uncertain nonlinear systems," *Automatica*, vol. 106, pp. 117–123, Aug. 2019.

[29] G. Zhu, J. Du, and Y. Kao, "Command filtered robust adaptive NN control for a class of uncertain strict-feedback nonlinear systems under input saturation," *J. Franklin Inst.*, vol. 355, no. 15, pp. 7548–7569, Oct. 2018.

[30] J. Yu, L. Zhao, H. Yu, and C. Lin, "Barrier Lyapunov functions-based command filtered output feedback control for full-state constrained nonlinear systems," *Automatica*, vol. 105, pp. 71–79, Jul. 2019.

[31] G. Cui, J. Yu, and Q. Wang, "Finite-time adaptive fuzzy control for MIMO nonlinear systems with input saturation via improved command-filtered backstepping," *IEEE Trans. Syst., Man, Cybern., Syst.*, early access, Aug. 6, 2020, doi: 10.1109/TSMC.2020.3010642.

[32] X. Li, L. Cao, X. Hu, and S. Zhang, "Command filtered model-free robust control for aircrafts with actuator dynamics," *IEEE Access*, vol. 7, pp. 139475–139487, 2019.
[33] H. Wang and S. Kang, "Adaptive neural command filtered tracking control for flexible robotic manipulator with input dead-zone," *IEEE Access*, vol. 7, pp. 22675–22683, 2019.
[34] J. Zhang, S. Li, C. K. Ahn, and Z. Xiang, "Decentralized event-triggered adaptive fuzzy control for nonlinear switched large-scale systems with input delay via command-filtered backstepping," *IEEE Trans. Fuzzy Syst.*, early access, Mar. 17, 2021, doi: 10.1109/TFUZZ.2021.3066297.
[35] Y. She, X. She, and M. E. Baran, "Universal tracking control of wind conversion system for purpose of maximum power acquisition under hierarchical control structure," *IEEE Trans. Energy Convers.*, vol. 26, no. 3, pp. 766–775, Sep. 2011.
[36] C. Treesatayapun and S. Uatrongjit, "Adaptive controller with fuzzy rules emulated structure and its applications," *Eng. Appl. Artif. Intell.*, vol. 18, no. 5, pp. 603–615, Aug. 2005.
[37] M. L. Buhl, "WT.PERF user's guide," Nat. Renew. Energy Lab., Golden, CO, USA, Tech. Rep., 2004.
[38] S. M. Muyeen, M. H. Ali, R. Takahashi, and T. Murata, "Comparative study on transient stability analysis of wind turbine generator system using different drive train models," *IET Renew. Power Gener.*, vol. 1, no. 2, pp. 131–141, 2007.
[39] W. Kwon and S. Won, "Uniformly ultimately boundedness stability condition of systems with state delay and input backlash," in *Proc. 14th Int. Conf. Control, Autom. Syst. (ICCAS)*, Gyeonggi-do, South Korea, Oct. 2014, pp. 1–5.
[40] C. Treesatayapun, "Knowledge-based reinforcement learning controller with fuzzy-rule network: Experimental validation," *Neural Comput. Appl.*, vol. 32, no. 13, pp. 9761–9775, Jul. 2020.
[41] J. J. Slotine and W. Li, *Apllied Nonlinear Control*. Upper Saddle River, NJ, USA: Prentice-Hall, 1991.
[42] K. Narendra and A. Annaswamy, "A new adaptive law for robust adaptation without persistent excitation," *IEEE Trans. Autom. Control*, vol. 32, no. 2, pp. 134–145, Feb. 1987.
[43] W. Deng and J. Yao, "Extended-state-observer-based adaptive control of electrohydraulic servomechanisms without velocity measurement," *IEEE/ASME Trans. Mechatronics*, vol. 25, no. 3, pp. 1151–1161, Jun. 2020.
[44] W. Deng and J. Yao, "Asymptotic tracking control of mechanical servosystems with mismatched uncertainties," *IEEE/ASME Trans. Mechatronics*, early access, Oct. 30, 2020.
[45] M. L. Fravolini, T. Yucelen, J. Muse, and P. Valigi, "Analysis and design of adaptive control systems with unmodeled input dynamics via multiobjective convex optimization," in *Proc. Amer. Control Conf. (ACC)*, Chicago, IL, USA, Jul. 2015, pp. 1579–1584.

MIAO HUANG received the Ph.D. degree in control theory and engineering from the East China University of Science and Technology, Shanghai, China, in 2015.

From 2017 to 2019, she was a Postdoctoral Fellow with the College of Control Science and Engineering, Zhejiang University, Hangzhou, China. She is currently with the College of Intelligent Manufacturing and Control Engineering, Shanghai Polytechnic University, Shanghai. She has published 15 international journal and conference papers and five patents for invention. She has taken charge of a Zhejiang Provincial Natural Science Foundation of China. Her research interests include adaptive control and dynamic wireless power transfer.

LILI TAO received the Ph.D. degree in control theory and engineering from the East China University of Science and Technology, Shanghai, China, in 2013.

Since 2013, she has been an Associate Professor with the College of Intelligent Manufacturing and Control Engineering, Shanghai Polytechnic University, Shanghai. She has published eight international articles and taken charge of three research projects on dynamic modeling and optimization control of typical chemical process. Her research interests include dynamic modeling of oxidation reaction of xylene and multi-objective and dynamic optimization in typical chemical production process.

ZHIHUA HU received the bachelor's and master's degrees in rail traction electrification and automation from Tongji University, Shanghai, China, in 1994 and 1998, respectively.

Since 1998, she has been with the College of Intelligent Manufacturing and Control Engineering, Shanghai Polytechnic University, Shanghai. She is currently the Head of the Department of Measurement, Control and Automation, Shanghai Polytechnic University. She has published three books, five patents, and more than ten international articles. She has been in charge of more than 20 research projects, including online remote monitoring of fan gearbox oil and fine filtration systems, and computer control systems for municipal waste treatment equipment.